

Proton–hydride tautomerism in hydrogen evolution catalysis

Luis M. Aguirre Quintana^{a,b}, Samantha I. Johnson^{a,b}, Sydney L. Corona^{a,b}, Walther Villatoro^{a,b}, William A. Goddard III^{a,b}, Michael K. Takase^{a,b}, David G. VanderVelde^{a,b}, Jay R. Winkler^{a,b,1}, Harry B. Gray^{a,b,1}, and James D. Blakemore^{a,b,c,1}

^aBeckman Institute, California Institute of Technology, Pasadena, CA 91125; ^bDivision of Chemistry and Chemical Engineering, California Institute of Technology, Pasadena, CA 91125; and ^cDepartment of Chemistry, University of Kansas, Lawrence, KS 66044

Contributed by Harry B. Gray, April 17, 2016 (sent for review February 4, 2016; reviewed by Alexander Miller and David Milstein)

Efficient generation of hydrogen from renewable resources requires development of catalysts that avoid deep wells and high barriers. Information about the energy landscape for H₂ production can be obtained by chemical characterization of catalytic intermediates, but few have been observed to date. We have isolated and characterized a key intermediate in 2e[−] + 2H⁺ → H₂ catalysis. This intermediate, obtained by treatment of Cp^{*}Rh(bpy) (Cp^{*}, η⁵-pentamethylcyclopentadienyl; bpy, κ²-2,2′-bipyridyl) with acid, is not a hydride species but rather, bears [η⁴-Cp^{*}H] as a ligand. Delivery of a second proton to this species leads to evolution of H₂ and reformation of η⁵-Cp^{*} bound to rhodium(III). With suitable choices of acids and bases, the Cp^{*}Rh(bpy) complex catalyzes facile and reversible interconversion of H⁺ and H₂.

rhodium | pentamethylcyclopentadienyl | catalysis | proton reduction | hydrogen evolution

Sustainable and economically competitive production of hydrogen (H₂) as a fuel depends on the development of new molecules and materials that catalyze conversion of protons and electrons into H₂ with high rates and minimal energy input (1). Platinum fulfills these latter requirements but fails the economic test. Rational design of new catalysts that overcome these challenges hinges on a detailed understanding of the elementary chemical reaction steps involved in H–H bond formation (2). Notably, catalysis with a molecular cobalt complex, a [BF₂]-bridged cobaloxime, has been shown by kinetics and modeling to proceed by protonation of a Co^{II}–H complex to yield H₂ (3). However, most intermediates in H₂ evolution elude detection, limiting insight into the bond-breaking and -making processes involved in catalysis (4). In recent work, we have descended to the second row of group 9 in the periodic table to enable observation and isolation of catalytic intermediates.

We report here on our investigations of [Cp^{*}Rh^{III}(diimine)L]²⁺ (Cp^{*}, η⁵-pentamethylcyclopentadienyl) complexes that evolve hydrogen catalytically on reduction. In early work, Kölle and Grätzel (5) found that H₂ is evolved on reduction at pH < 2 in an aqueous photochemical system, and Deronzier and coworkers (6) observed electrochemical H₂ evolution at pH 1. Of interest here is our finding that H₂ is evolved electrochemically in acetonitrile solutions of [Cp^{*}Rh^{III}(diimine)L]²⁺ with tosic acid serving as the proton source (7). The η⁵-Cp^{*} ligand imparts high stability and solubility to these catalysts (8). Not surprisingly, then, they have been used widely for catalysis of redox transformations, including reduction of NAD⁺ to NADH (9–11), dehydrogenation of formic acid or alcohols (12, 13), and hydrogenation of organic compounds (14). In these reactions, Rh^{III}–H is believed to be a reactive intermediate (15).

Hydrogen evolution catalysts have been discovered recently in which the metal center and associated ligands cooperate in unexpected ways. A case in point features ligand-centered protonation and subsequent hydride-like reactivity of a nascent C–H bond in a nickel phlorin system (16), although a nickel hydride was not implicated in the cycle for hydrogen evolution. In other work of note, Hull et al. (17) reported dehydrogenation of HCO₂H promoted by proton-responsive hydroxybipyridine-ligated catalysts, and Lacy et al. (18) showed that ligand-centered protonation of a cobalt complex could lead to hydrogen evolution.

Much work has been done on Cp^{*}Rh compounds. Of importance is that Maitlis and coworkers (19) reported Cp^{*}Rh(Cp^{*}H) formation in low yield (14%) by reduction of [(Cp^{*})₂Rh](PF₆). In other relevant work, Jones et al. (20) showed that the dihydride complex Cp^{*}Rh(PMe₃)(H)₂ loses free Cp^{*}H on treatment with excess PMe₃ at elevated temperature. Also, several other rhodium and iron complexes with Cp^{*}H ligands are known (21–25).

Building on these earlier investigations, we report here an unusual mode of metal–ligand cooperation that drives proton–hydride tautomerization during hydrogen evolution. We have found that η⁴-Cp^{*}H is produced en route to H₂ production with Cp^{*}Rh(diimine) complexes, suggesting an important role for ligand participation in hydrogen evolution catalysis.

Results

The preparation, isolation, and crystallographic characterization of Cp^{*}Rh^I(diimine) complexes with η⁵-Cp^{*} and κ²-diimine coordination are all well-documented (26, 27). Treatment of the κ²-2,2′-bipyridyl [bpy; Cp^{*}Rh(bpy); **1**] (Fig. 1) and 1,10-phenanthroline [phen; Cp^{*}Rh(phen); **2**] complexes with excess protonated dimethylformamide ([DMF-H]⁺[OTf][−]) in MeCN (pK_a = 6.1) results in stoichiometric production of H₂ gas. Use of weaker acids lowers the thermodynamic driving force for hydrogen evolution (28), likely slowing the reaction and increasing the chance of trapping one or more intermediates. Treatment of **1** with one to five equivalents of [Et₃NH]⁺Br[−] (pK_a = 18.8) in CD₃CN results in a rapid color change

Significance

The discovery of efficient hydrogen evolution catalysts for solar fuels production continues to be an active research field. Catalyst optimization depends on detailed knowledge of the elementary chemical reaction steps involved in catalysis. Isolation of intermediates in catalytic processes is uncommon owing to their necessarily low stability. By using weak acids, we have isolated and characterized an intermediate in the 2e[−] + 2H⁺ → H₂ reaction catalyzed by η⁵-pentamethylcyclopentadienyl (Cp^{*}) Rh(κ²-2,2′-bipyridyl) [Rh(bpy)]. We find that the preferred site of Cp^{*}Rh(bpy) protonation is not the metal center but is the Cp^{*} ligand. Despite the reputation of Cp^{*} as a stable ligand in organometallic chemistry, these results suggest an important role for close metal–ligand cooperation in promoting hydrogen–evolution catalysis.

Author contributions: S.I.J., D.G.V., J.R.W., H.B.G., and J.D.B. designed research; L.M.A.Q., S.I.J., S.L.C., W.V., M.K.T., and J.D.B. performed research; W.A.G. contributed new reagents/analytic tools; L.M.A.Q., S.I.J., S.L.C., W.V., M.K.T., D.G.V., J.R.W., H.B.G., and J.D.B. analyzed data; and S.I.J., J.R.W., H.B.G., and J.D.B. wrote the paper.

Reviewers: A.M., University of North Carolina; and D.M., The Weizmann Institute of Science.

The authors declare no conflict of interest.

Data deposition: The atomic coordinates and structure factors have been deposited in the Cambridge Crystallographic Data Centre (accession no. 1424707).

¹To whom correspondence may be addressed. Email: winklerj@caltech.edu, hbgray@caltech.edu, or blakemore@ku.edu.

This article contains supporting information online at www.pnas.org/lookup/suppl/doi:10.1073/pnas.1606018113/-DCSupplemental.

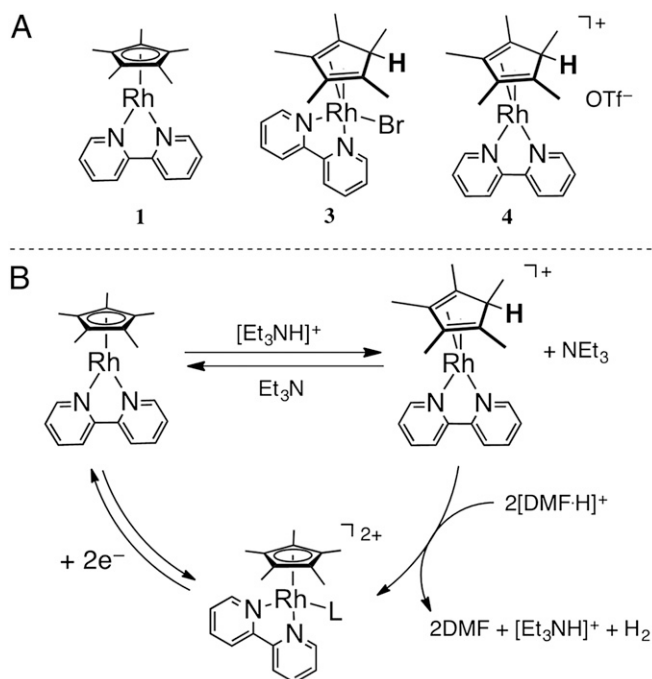


Fig. 1. (A) Structures of **1**, **3**, and **4**. (B) Proposed cycle for H_2 evolution catalyzed by **1** through a $[\text{Cp}^*\text{H}]\text{Rh}$ complex.

from purple to reddish brown but no gas evolution, consistent with formation of compound **3** (Fig. 1). Similar spectral features are encountered on treatment of **1** or **2** with $[\text{Et}_3\text{NH}]^+\text{OTf}^-$, resulting in formation of analogous compounds **4** (with bpy) and **5** (with phen) bearing the $[\text{Cp}^*\text{H}]$ ligand.

Allowing a concentrated acetonitrile solution of **3** to stand for several days yielded orange–yellow single crystals suitable for X-ray diffraction (the structure that we obtained is shown in Fig. 2). The geometry at the Rh^{I} center is distorted square pyramidal, with a mirror plane containing the Rh1-Br1 bond bisecting the molecule. A proton (observable in the electron density map) is present on the ring of the former Cp^* ligand, with the $[\text{Cp}^*\text{H}]$ bound in an η^4 mode. The bpy ligand retains typical κ^2 coordination in accordance with our interpretation of its ^1H and ^{13}C NMR spectra. The Rh1-N1 bond length is 2.117(1) Å, whereas Rh1-C2 and Rh1-C3 are 2.133(1) and 2.112(2) Å, respectively. The mirror plane symmetry element requires identical bond distances from Rh1 to the corresponding N1' , C2' , and C3' atoms.[†]

In **1**, the C–C bond length of 1.422(4) Å between the pyridyl rings of the bpy ligand is consistent with considerable bpy anion character (29) caused by electron donation from Rh^{I} augmented by the strongly π -donating $\eta^5\text{-Cp}^*$ ligand. On protonation of Cp^* to form **3**, this C–C bond lengthens to 1.475(3) Å, similar to the distance found in free bpy and notably, an analogous $[\text{Cp}^*\text{Rh}^{\text{III}}(\text{bpy})\text{Cl}]\text{Cl}$ complex (30). This marked structural change is attributable to the conversion of the π -donating $[\eta^5\text{-Cp}^*]^-$ ligand to a π -accepting $[\eta^4\text{-Cp}^*\text{H}]^0$ group. In the crystal structure of a free Cp^*H analog,

$\text{Cp}(\text{CH}_2\text{Ar})_5\text{H}$ [$\text{Ar} = -(\text{C}_6\text{H}_4)\text{CH}_3$], the corresponding C2–C3 bond length is 1.343(3) Å, and the C3–C3' bond is 1.467(3) Å (31). In **3**, the C2–C3 and C3–C3' bonds are nearly identical at 1.442(2) and 1.442(3) Å, respectively, consistent with both σ -donation and π -backbonding between Rh^{I} and $[\text{Cp}^*\text{H}]$.

Electronic absorption spectra reflect the marked change in electronic structure on protonation of **1** to form **3**. Bands in the visible region ($\epsilon \sim 4\text{--}15 \times 10^3 \text{ M}^{-1} \text{ cm}^{-1}$) assigned to metal-to-ligand charge-transfer (MLCT) transitions (27, 32) dominate the spectrum of **1**, accounting for its purple color. Conversely, the spectrum of **3** displays intense bands ($\epsilon \sim 20\text{--}30 \times 10^3 \text{ M}^{-1} \text{ cm}^{-1}$) across the UV region with weaker absorption tailing into the visible ($\epsilon \sim 1.7 \times 10^3 \text{ M}^{-1} \text{ cm}^{-1}$ at 507 nm), producing a reddish brown solution. The UV absorption in **3** is attributable to both intraligand and MLCT transitions. The observed blue shift of MLCT absorption bands is consistent with a positive shift of the rhodium(II/I) formal potential on shifting coordination from the electron-donating $[\eta^5\text{-Cp}^*]^-$ ligand to the π -accepting $[\eta^4\text{-Cp}^*\text{H}]$ group. Similarly, $\text{Rh}(\text{norbornadienyl})(\text{bpy})\text{Cl}$ is a reddish solid exhibiting only weak visible absorption ($\epsilon \sim 0.85 \times 10^3 \text{ M}^{-1} \text{ cm}^{-1}$ at 478 nm) (33), and $[\text{Rh}(\text{CO})_2(\text{bpy})]\text{ClO}_4$ is a yellow solid (34). Because most $[\text{Cp}^*\text{Rh}^{\text{III}}(\text{diimine})\text{L}]^{2+}$ complexes are pale yellow to orange in appearance, the coloration of **3** more closely resembles that of an Rh^{III} compound, although it is formally Rh^{I} (5, 7). This finding raises the possibility that compounds protonated at Cp^* may have escaped detection in the past, because their UV-visible absorption profiles are not markedly different from spectra of their hydride analogs.

Exposure of **3**, **4**, and **5** to excess Et_3NH^+ does not lead to additional protonation of the Rh complex or any other transformation. Treatment with stronger acid ($[\text{DMF-H}]^+[\text{OTf}]^-$), however, triggers quantitative H_2 evolution and generation of Rh^{III} . For example, addition of 1 eq $[\text{NEt}_3\text{H}]^+[\text{OTf}]^-$ to 50 mg **2** results in negligible H_2

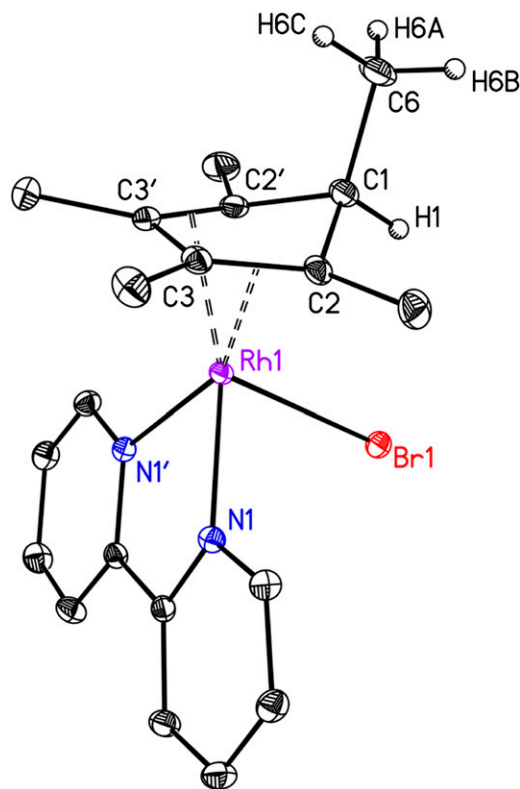


Fig. 2. Structure of **3**. Displacement ellipsoids are shown at 50% probability. One cocrystallized acetonitrile molecule and all H atoms, except those bonded to C1 and C6, are omitted for clarity. Blue, nitrogen; purple, rhodium; red, bromide.

[†]The distinctive ^1H NMR spectrum of **3** is characterized by two singlets in the alkyl region (1.85 and 0.94 ppm) along with a doublet and quartet ($d = 0.54$; $q = 2.54$ ppm; $^3J_{\text{H-H}} = 6.2$ Hz). The relative integrations (6:6:3:1, respectively) of these peak groups are consistent with $[\text{Cp}^*\text{H}]$ coordinated to Rh^{I} . Resonances in the aromatic region shift on conversion of **1** to **3** but retain the expected couplings for an intact bpy ligand. The remaining features in the ^1H NMR spectrum of **3** are attributed to excess $[\text{Et}_3\text{NH}]^+\text{Br}^-$ and residual CH_3CN . Coordination of $[\text{Cp}^*\text{H}]$ to Rh is confirmed by comparison with the ^1H NMR of the free ligand ($\delta = 1.74$ and 1.79 ppm; $d = 0.97$; $q = 2.45$ ppm; $^3J_{\text{H-H}} = 7.6$ Hz) as well as the $^{13}\text{C}\{^1\text{H}\}$ NMR of **3** [$d = 94.4$ ppm; $^1J_{\text{Rh-C}} = 10.6$ Hz; $d = 55.4$ ppm; $^1J_{\text{Rh-C}} = 10.9$ Hz; $d = 57$ ppm; $^2J_{\text{Rh-C}} = 3.6$ Hz; $^{103}\text{Rh}(I = 1/2)$ is 100% abundant].

at 238 K (24). Our isolation and characterization of **4**, however, raise the possibility of an alternative pathway (B in Fig. 4), in which Cp*H serves as a proton relay (37): protonation of **4** at the metal center would form $[(\text{Cp}^*\text{H})\text{Rh}(\text{H})(\text{bpy})]^{2+}$, which then could evolve H_2 through intramolecular reductive elimination. Protonation of **4** at the Rh center is consistent with the d_{z^2} -localized HOMO identified in DFT calculations. The fact that Et_3NH^+ cannot drive this reaction at low concentrations is attributable to the decreased basicity of **4**; use of stronger acid ($[\text{DMF-H}]^+$) leads to rapid H_2 generation. The intramolecular reductive elimination mechanism is analogous to pathways proposed to be operative in other highly active H_2 evolution catalysts; the search for experimental evidence for these pathways remains an active area of investigation (38–40).

In our case, $[\text{Cp}^*\text{H}]$ does not dissociate from the metal center, and quantitative H_2 evolution proceeds from the reduced complex (21). Importantly, $\eta^5\text{-Cp}^*$ coordination to Rh is restored after hydrogen evolution. The unique properties of the Cp* ligand framework enable π -donor $[\eta^5\text{-Cp}^*]$ to convert reversibly to π -acceptor $[\eta^4\text{-Cp}^*\text{H}]^0$, stabilizing intermediates in the catalytic cycle. Furthermore, this transformation places a proton tantalizingly close to the metal center (41, 42). For $[\text{Cp}^*\text{Rh}]$ bearing $\kappa^2\text{-(C,N)-2-phenylpyridine}$ (ppy), Norton and coworkers (43) have shown that an $\text{Rh}^{\text{III}}\text{-H}$ is the preferred form, likely because of the more electron-rich metal center. However, the $\text{Rh}^{\text{III}}/[\text{Cp}^*\text{Rh}^{\text{III}}(\text{ppy})(\text{CH}_3\text{CN})^+/\text{Cp}^*\text{Rh}^{\text{I}}(\text{ppy})^-]$ potential in the ppy complex is ~ 500 mV more negative than that of **1**, resulting in a barrier that prevents H_2 -driven production of $[\text{Cp}^*\text{Rh}(\text{ppy})^-]$ with NEt_3 as base (44).

In $\text{Cp}^*\text{Rh}(\text{diimine})$ complexes, the metal center seems to act as the primary site of proton capture from solution, initially forming a hydride species (**4H**) that we do not directly detect. This hydride then tautomerizes by proton transfer to the nearby basic $[\text{Cp}^*]^-$ ligand, restoring the formal Rh^{I} oxidation state on formation of **4**. This proton-hydride tautomerism represents an interesting analog to proton capture mechanisms in other complexes, such as those described by DuBois and coworkers (38), which rely on pendant amine bases to shuttle protons to the metal center. Our case also contrasts with older reports from Davies et al. (45), Reger et al. (46), and Norton and coworkers (47) involving direct *exo*-transfer of $[\text{H}^-]$ to a Cp ligand bound to iron or tungsten complexes.

The pathway of H_2 generation involving initial protonation of complex **4** and subsequent H–H bond formation is reminiscent of bond activation by close metal–ligand cooperation (48), especially those cases involving ligand dearomatization–aromatization processes in pincer-type systems (49). Milstein and coworkers (50) have observed proton transfer to and from a pincer arm in an Ru–H complex, resulting in aromatization–dearomatization of a pyridine core on the ligand. Additionally, in a related example, an Ir complex was suggested to react with D_2 through initial dearomatization of a pincer ligand (51). It follows that the specific organic acid–base used with the complexes described here could affect the energetics

and preference of the reaction channel through hydrogen-bonding interactions. In the case of **4**, proton transfer from $[\text{Cp}^*\text{H}]$ to form H_2 would result in aromatization of the $[\text{Cp}^*]$; this energetically favorable process lowers the barrier to H–H bond formation.

Hydrogen evolution catalysts must assemble two electrons and two protons into an H_2 molecule. The order in which these four particles are delivered to the catalyst impacts the speed and energetics of the transformation. In the case of $[\text{Cp}^*\text{Rh}^{\text{III}}(\text{diimine})\text{L}]^{2+}$ catalysts, the sequence is $e^- + e^- + \text{H}^+ + \text{H}^+$. Owing to the instability of the Rh^{II} oxidation state, the second electron is delivered at a more positive potential than the first electron. The energetics of subsequent proton delivery, however, follow the usual trend, wherein the first proton can be delivered by a relatively weak acid, but a stronger acid is required to deliver the second proton. After the second proton has been delivered to **4** or **4H**, the complex is poised to facilitate H–H bond formation followed by H_2 dissociation. Our findings provide key insight into the design elements required for a catalyst that avoids deep wells and high barriers in $2e^- + 2\text{H}^+$ hydrogen evolution.

Materials and Methods

All manipulations were carried out in a dry N_2 -filled glovebox (Vacuum Atmospheres Co.) or under N_2 atmosphere using standard Schlenk techniques unless otherwise noted. All solvents were of commercial grade and dried over activated alumina using a J. C. Meyer Solvent Purification System before use. All chemicals were from major commercial suppliers and used as received without additional purification. ^1H , ^{13}C , and ^{19}F NMR spectra were collected on 400- or 500-MHz Varian or Bruker Spectrometers and referenced to the residual protiosolvent signal (52) in the case of ^1H and ^{13}C or the deuterium lock signal in the case of ^{19}F . Chemical shifts (δ) are reported in units of parts per million, and coupling constants (J) are reported in hertz.

$\text{Cp}^*\text{Rh}(\text{bpy})$ and $\text{Cp}^*\text{Rh}(\text{phen})$ were synthesized according to the literature method using $\text{Na}(\text{Hg})$ ²⁷. $[\text{DMF-H}]^+\text{OTf}^-$ was synthesized according to the method by Favier and Duñach (53). $[\text{Et}_3\text{NH}]^+\text{OTf}^-$ was prepared according to the literature (54). The rhodium complexes bearing Cp^*H were not isolated in pure form, but instead generated in situ by treatment with triethylammonium salts. ^1H NMR, $^{13}\text{C}\{^1\text{H}\}$ NMR, and electronic absorption spectroscopy were used to confirm clean conversion of the rhodium starting materials. In one case (**3**), crystals suitable for X-ray diffraction were obtained as described below.

(Cp*H)(bpy)Br (3). In a typical experiment, ~ 5 mg **1** was dissolved in acetonitrile, and then, ~ 1 –5 eq $[\text{Et}_3\text{NH}]^+\text{Br}^-$ was added, resulting in a color change from purple to brown and quantitative formation of **3**. The resulting solution contains **3** plus the conjugate base NEt_3 and any excess $[\text{Et}_3\text{NH}]^+\text{Br}^-$. For NMR analysis, the compound was prepared in $d_3\text{-MeCN}$ and transferred to a J. Young Tube. No decomposition of the compound over hours was detectable. However, **3** was prepared fresh for each experiment and typically not isolated as a solid.

Peak multiplicities for the NMR spectra are listed, where d is doublet, q is quartet, s is singlet, dd is doublet of doublets, td is triplet of doublets, t is triplet, and ddd is doublet of doublet of doublets.

^1H NMR (400 MHz; $\text{MeCN-}d_3$) δ 8.88 (d, 2H, $^3J_{\text{H-H}} = 5.1$ Hz), 8.28 (d, 2H, $^3J_{\text{H-H}} = 8.2$ Hz), 8.02 (td, 2H, $^3J_{\text{H-H}} = 7.9$ Hz, $^4J_{\text{H-H}} = 1.6$ Hz), 7.59 (t, 2H, $^3J_{\text{H-H}} = 6.4$ Hz),

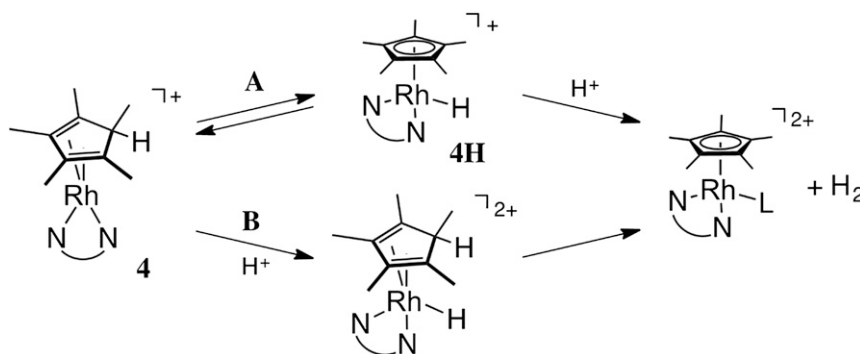


Fig. 4. Proposed pathways for hydrogen evolution starting from **4**.

21. Macias R, et al. (1997) Effects of metal-centre orbital control on cluster character and electron distribution between borane and hydrocarbon ligands; significance of the structures of $[\mu-9,10-(\text{SMe})-8,8-(\text{PPh}_3)_2\text{-nido-}8,7\text{-IrSB}_9\text{H}_9]$ and $[\mu-9,10-(\text{SMe})-8-(\eta^4\text{-C}_5\text{Me}_5\text{H})\text{-nido-}8,7\text{-RhSB}_9\text{H}_9]$. *J Chem Soc Dalton Trans* (2):149–152.
22. Zamorano A, Rendón N, Valpuesta JEV, Álvarez E, Carmona E (2015) Synthesis and reactivity toward H_2 of $(\eta^5\text{-C}_5\text{Me}_5)\text{Rh}(\text{III})$ complexes with bulky aminopyridinate ligands. *Inorg Chem* 54(13):6573–6581.
23. Enders M, et al. (2002) Coordination chemistry of neutral quinolyl- and aminophenylcyclopentadiene derivatives. *J Organomet Chem* 641(1–2):81–89.
24. Tsai W-M, Rausch MD, Rogers RD (1996) Improved synthesis of pentabenzylcyclopentadiene and study of the reaction between pentabenzylcyclopentadiene and iron pentacarbonyl. *Organometallics* 15(11):2591–2594.
25. Liu L-K, Luh L-S (1996) Consecutive butylations on the cyclopentadienyl ring of the $[(\eta^5\text{-C}_5\text{H}_5)\text{Fe}(\text{CO})_2\text{PPh}_3]^+$ cation. *Organometallics* 15(25):5263–5265.
26. Blakemore JD, et al. (2014) Pentamethylcyclopentadienyl rhodium complexes. *Polyhedron* 84:14–18.
27. Nakai H, Jeong K, Matsumoto T, Ogo S (2014) Catalytic C-F bond hydrogenolysis of fluoroaromatics by. *Organometallics* 33(17):4349–4352.
28. Appel AM, Helm ML (2014) Determining the overpotential for a molecular electrocatalyst. *ACS Catal* 4(2):630–633.
29. Gore-Randall E, Irwin M, Denning MS, Goicoechea JM (2009) Synthesis and characterization of alkali-metal salts of 2,2'- and 2,4'-bipyridyl radicals and dianions. *Inorg Chem* 48(17):8304–8316.
30. Dadci L, et al. (1995) π -Arene aqua complexes of cobalt, rhodium, iridium, and ruthenium: Preparation, structure, and kinetics of water exchange and water substitution. *Inorg Chem* 34(1):306–315.
31. Schumann H, Sührling K, Weimann R, Hummert M (2000) Deca(4-methylbenzyl)ferrocene and -stannocene. *Z Naturforsch B* 60(6):527–532.
32. Ladwig M, Kaim W (1992) Electronic structure of catalytic intermediates for production of H_2 : $(\text{C}_5\text{Me}_5)\text{Ir}(\text{bpy})$ and its conjugated acid. *J Organomet Chem* 439(1):79–90.
33. Robertson JJ, Kadziola A, Krause RA, Larsen S (1989) Preparation and characterization of four- and five-coordinate rhodium(I) complexes. Crystal structures of chloro(2-phenylazo)pyridine(norbornadiene)rhodium(I), (2,2'-bipyridyl)(norbornadiene)rhodium(I) chloride hydrate, and chloro(2,2'-bipyridyl)(norbornadiene)rhodium(I). *Inorg Chem* 28(11):2097–2102.
34. Reddy GKN, Susheelamma CH (1970) 2,2'-Bipyridyl and o-phenanthroline carbonyl complexes of rhodium. *J Chem Soc D* (1):54.
35. Roberts JAS, Bullock RM (2013) Direct determination of equilibrium potentials for hydrogen oxidation/production by open circuit potential measurements in acetonitrile. *Inorg Chem* 52(7):3823–3835.
36. Pitman CL, Finster ON, Miller AJ (March 7, 2016) Cyclopentadiene-mediated hydride transfer from rhodium complexes. *Chem Commun*, 10.1039/C6CC00575F.
37. Kefalidis CE, et al. (2015) Can a pentamethylcyclopentadienyl ligand act as a proton-relay in f-element chemistry? Insights from a joint experimental/theoretical study. *Dalton Trans* 44(6):2575–2587.
38. Wilson AD, et al. (2006) Hydrogen oxidation and production using nickel-based molecular catalysts with positioned proton relays. *J Am Chem Soc* 128(1):358–366.
39. Jacques P-A, Artero V, Pécaut J, Fontecave M (2009) Cobalt and nickel diimine-dioxime complexes as molecular electrocatalysts for hydrogen evolution with low overvoltages. *Proc Natl Acad Sci USA* 106(49):20627–20632.
40. Solis BH, et al. (2014) Theoretical analysis of cobalt hangman porphyrins: Ligand dearomatization and mechanistic implications for hydrogen evolution. *ACS Catal* 4(12):4516–4526.
41. Helm ML, Stewart MP, Bullock RM, DuBois MR, DuBois DL (2011) A synthetic nickel electrocatalyst with a turnover frequency above 100,000 s^{-1} for H_2 production. *Science* 333(6044):863–866.
42. Solis BH, Yu Y, Hammes-Schiffer S (2013) Effects of ligand modification and protonation on metal oxime hydrogen evolution electrocatalysts. *Inorg Chem* 52(12):6994–6999.
43. Hu Y, et al. (2012) Synthesis, electrochemistry, and reactivity of new iridium(III) and rhodium(III) hydrides. *Organometallics* 31(14):5058–5064.
44. Hu Y, Norton JR (2014) Kinetics and thermodynamics of H^+/H^* transfer from a rhodium(III) hydride. *J Am Chem Soc* 136(16):5938–5948.
45. Davies SG, Hibberd J, Simpson SJ, Thomas SE, Watts O (1984) Carbon monoxide reduction. Carbonyl(η^5 -cyclopentadienyl)hydrido[1,2-bis(diphenylphosphino)ethane]iron: Reactions and formation by reduction of the complex $[(\eta^5\text{-C}_5\text{H}_5)\text{Fe}(\text{Ph}_2\text{PCH}_2\text{CH}_2\text{PPh}_2)(\text{CO})]\text{PF}_6$. *J Chem Soc Dalton Trans* (4):701–709.
46. Reger DL, Belmore KA, Atwood JL, Hunter WE (1983) The cis addition of hydride to η^2 -alkyne complexes by initial reaction at an η^5 -cyclopentadienyl ($\eta^5\text{-C}_5\text{H}_5$) ring. Crystal and molecular structure of the carbonyl- η^5 -cyclopentadienyliron complex ($\eta^5\text{-C}_5\text{H}_5$) $\text{FeCO}(\text{PPh}_3)$. *J Am Chem Soc* 105(17):5710–5711.
47. Bullock RM, Headford CEL, Kegley SE, Norton JR (1985) Hydrogen exchange between the methyl and hydride ligands of dicyclopentadienylhydridomethyltungsten prior to methane elimination. *J Am Chem Soc* 107(3):727–729.
48. Khushnudinova JR, Milstein D (2015) Metal-ligand cooperation. *Angew Chem Int Ed Engl* 54(42):12236–12273.
49. Zhang J, Leitun G, Ben-David Y, Milstein D (2005) Facile conversion of alcohols into esters and dihydrogen catalyzed by new ruthenium complexes. *J Am Chem Soc* 127(31):10840–10841.
50. Zhang J, Gandelman M, Shimon LJW, Rozenberg H, Milstein D (2004) Electron-rich, bulky ruthenium PNP-type complexes. Acceptorless catalytic alcohol dehydrogenation. *Organometallics* 23(17):4026–4033.
51. Ben-Ari E, Leitun G, Shimon LJW, Milstein D (2006) Metal-ligand cooperation in C-H and H_2 activation by an electron-rich PNP Ir(I) system: Facile ligand dearomatization-aromatization as key steps. *J Am Chem Soc* 128(48):15390–15391.
52. Fulmer GR, et al. (2010) NMR chemical shifts of trace impurities: Common laboratory solvents, organics, and gases in deuterated solvents relevant to the organometallic chemist. *Organometallics* 29(9):2176–2179.
53. Favier I, Duñach E (2004) New protic salts of aprotic polar solvents. *Tetrahedron Lett* 45(17):3393–3395.
54. Fumino K, Fossog V, Wittler K, Hempelmann R, Ludwig R (2013) Dissecting anion-cation interaction energies in protic ionic liquids. *Angew Chem Int Ed Engl* 52(8):2368–2372.
55. Sheldrick GM (1990) Phase annealing in SHELX-90: Direct methods for larger structures. *Acta Crystallogr A* 46(6):467–473.
56. Sheldrick GM (2008) A short history of SHELX. *Acta Crystallogr A* 64(Pt 1):112–122.
57. Müller P (2009) Practical suggestions for better crystal structures. *Crystallogr Rev* 15(1):57–83.
58. Becke AD (1993) Density-functional thermochemistry. III. The role of exact exchange. *J Chem Phys* 98(7):5648–5652.
59. Lee C, Yang W, Parr RG (1988) Development of the Colle-Salvetti correlation-energy formula into a functional of the electron density. *Phys Rev B Condens Matter* 37(2):785–789.
60. Franci MM, et al. (1982) Self-consistent molecular orbital methods. XXIII. A polarization-type basis set for second-row elements. *J Chem Phys* 77(7):3654–3665.
61. Hehre WJ, Ditchfield R, Pople JA (1972) Self-consistent molecular orbital methods. XII. Further extensions of Gaussian-type basis sets for use in molecular orbital studies of organic molecules. *J Chem Phys* 56(5):2257–2261.
62. Hay PJ, Wadt WR (1985) Ab initio effective core potentials for molecular calculations. Potentials for potassium to gold including the outermost core orbitals. *J Chem Phys* 82(1):299–310.
63. Zhao Y, Truhlar DG (2008) The M06 suite of density functionals for main group thermochemistry, thermochemical kinetics, noncovalent interactions, excited states, and transition elements: Two new functionals and systematic testing of four M06-class functionals and 12 other functionals. *Theor Chem Acc* 120(1–3):215–241.
64. Martin JML, Sundermann A (2001) Correlation consistent valence basis sets for use with the Stuttgart-Dresden-Bonn relativistic effective core potentials: The atoms Ga-Kr and In-Xe. *J Chem Phys* 114(8):3408–3420.
65. Bridgeman OC, Aldrich EW (1964) Vapor pressure tables for water. *J Heat Transfer* 86(2):279–286.
66. Kelly CP, Cramer CJ, Truhlar DG (2007) Single-ion solvation free energies and the normal hydrogen electrode potential in methanol, acetonitrile, and dimethyl sulfoxide. *J Phys Chem B* 111(2):408–422.
67. Lam YC, Nielsen RJ, Gray HB, Goddard WA (2015) A Mn bipyrimidine catalyst predicted to reduce CO_2 at lower overpotential. *ACS Catal* 5(4):2521–2528.
68. Bochevarov AD, et al. (2013) Jaguar: A high-performance quantum chemistry software program with strengths in life and materials sciences. *Int J Quantum Chem* 113(18):2110–2142.
69. Zhao Y, Truhlar DG (2009) Benchmark energetic data in a model system for Grubbs II Metathesis Catalysis and Their Use for the Development, Assessment, and Validation of electronic structure methods. *J Chem Theory Comput* 5(2):324–333.
70. Young KJH, et al. (2011) Synthesis of osmium and ruthenium complexes bearing dimethyl (S,S)-2,2'-(pyridine-2,6-diyl)-bis-(4,5-dihydrooxazol-4-carboxylate) ligand and application to catalytic H/D exchange. *J Mol Catal A: Chem* 339(1–2):17–23.